Applying MIMO concept to time reversal method on target resolving in shallow water

Jingning Jiang, Xiang Pan*, Zheng Zheng
College of Information Science & Electronic Engineering, Zhejiang University, Hangzhou(310027), China
*Corresponding author: panxiang@zju.edu.cn

***Abstract*—In underwater target detection, time reversal method shows its ability to suppress interference and focus energy in a complicated environment. For better sonar detection performance, we borrow the multiple-input-multiple-output structure and apply this concept into time reversal sonar detection. By deploying multiple source/receive arrays, this widely-space detection configuration brings a more accurate or reliable result, by exploiting diversities and data fusion. A TR-MIMO sonar detection scheme is discussed here. Also, preliminary simulation and experiment using two source/receive arrays were conducted and figured out a target with a reliable estimation. A better result will be achieved when using more sophisticated methods as detailed discussion,**

***Index Terms*—TR-MIMO, Shallow Water, Target detection, Active Sonar.**

I. Introduction

Harbor and littoral area security is a big issue worldwide, which is preventing intruders, such as divers or underwater vehicles from posing threats, even severe damages. These slowly moving targets are always remaining acoustic silent, thus only active detection can be reliable for coastal assets protection. However, in shallow water, the high level reverberation returns mask the dispersive echo from targets of interest, making the detection work a tougher one. This indicates a focus wave or narrow beam is needed for active detection. As well known to all, time reversal (TR) or phase conjugation method has long been tested and proven as a robust tool to focus wave and energy in space and time. Time reversal method in target detection evolves into two different ways, that iterative TR (ITR) [1] and decomposition-of-time-reversal-operator (DORT) [2], performing selective focus in a reverberant and multiple scatterers environment. Except static target detection, time reversal method shows its potential of slowly moving targets undergoing some displacements in laboratory ultrasonic scale [3]. But in actual field tests, time reversal is limited by time varying ocean environment, making a stable focus impossible during tens of minutes. At the meantime, phase perturbations and small changes in ocean waveguide can cause severe mismatch. Thus, sensitive kernel [4] is used to mitigate this issue, as well as to identify, even locate these changes. But it is far beyond our consideration in this paper.

Moreover, we try to utilize multiple-input-multiple-output (MIMO) system to enhance detection performance. MIMO concept has been introduced from communication society to target detection fields. But the fast growing MIMO detection framework mainly thrives in radar regime. Though a MIMO detection system exploits all the possible diversities in specific scenarios, it drops the coherent gain as a trade-off, meaning a lower signal-to-noise/interference ratio at receiver end. However, the propagation effects (such as time-delay spread) in underwater acoustic channel lead to a tough work to mitigate mutual interference [5] and echo separation. We can still borrow some insights from MIMO concept to enhance active sonar performance [6] and achieve high resolution results [7]. Here, we propose to use multiple vertical source/receive array (SRA), utilizing the orthogonal signals and multiple decisions to better resolve a target. Further, target's more accurate relative position can be acquired by simple data fusion.

In this paper, we first discuss the TR-MIMO detection framework, and its signal model analysis. Some preliminary experiment results were gathered at a 20-m depth lake in 2013, as analyzed in the third section. Finally, the conclusion is drawn on the theoretic and experimental performance.

II. TR-MIMO Detection

A. Time Reversal Method

First, we consider a signal model for a M-element SRA in a multiple scatterers environment. The procedure of one data acquisition at each transmission is, first using a set of elements transmit sequence(s), for example $s(t)$, then each element switches to receiving cycle to record signals. Thus a time domain recorded signal, which is transmitted from the mth element and received at the nth element, comes as $p(z_m, z_n, t)$ (z_m is the depth corresponding to the mth element of SRA). Because the data is gathered in a multiple scatterers environment, $p(z_m, z_n, t)$ is associated with K point scatters, with kth point scatterer's reflection characteristic is described by $a_k(t)$ at range r_k. Thus it gives

$$p(z_m, z_n, t) = \sum_{k=1}^{K} s(t) * g(z_m, z_k, r_k, t) * a_k(t) * g(z_k, z_n, r_k, t) + n(z_n, t), \tag{1}$$

where $*$ denotes the convolution operator, $g(z_s, z_r, r, t)$ is the time domain Green's function between source depth z_s to receive depth z_r at range r, and $n(z_n, t)$ represents the noise on the nth element. If the Green's function, scatterer's reflection, and noise process in (1) are assumed time-invariant or ergodic, $p(z_m, z_n, t)$'s frequency counterpart can be formulated through

978-0-933957-43-5 ©2015 MTS

Fourier transformation as:

$$P(z_m, z_n, f) = \sum_{k=1}^{K} S(f)G(z_m, z_k, r_k, f)A_k(f) \times G(z_k, z_n, r_k, f) + N(z_n, f). \tag{2}$$

In a next cycle, the transmitted signal is based on the time reversed version of the last received signal $r(t)$, taking $s_{TR}(t) = r^*(-t)$ as a simple instance. Following the same procedure described above, we only need to replace $s(t)$ with $s_{TR}(t)$, thus leading to the final received echo $x(t)$ for detection. The convolution result in nth element for $\mathbf{x}(t)$ and its frequency response $\mathbf{X}(f)$ has components as

$$x(z_m, z_n, t) = \sum_{k=1}^{K} s^*(-t) * g_f(z_m, z_k, r_k, t) * a_k(t) * g_b(z_k, z_n, r_k, t) + n(z_n, t), \quad \text{and} \tag{3}$$

$$X(z_m, z_n, f) = \sum_{k=1}^{K} S^*(f)G_f(z_m, z_k, r_k, f)A_k(f) \times G_b(z_k, z_n, r_k, f) + N(z_n, f). \tag{4}$$

In (3), $g_f(z_m, z_k, r_k, t)$ represents the correlation of forward propagation function, and $g_b(z_k, z_n, r_k, t)$ is the correlation of backward propagation from scatterers to SRA. $G_f(z_m, z_k, r_k, f)$ and $G_b(z_k, z_n, r_k, f)$ are their Fourier transformation. Their mathematic forms is given in detailed as

$$\begin{aligned} g_f(z_m, z_k, r_k, t) &= g(z_m, z_k, r_k, t) * g^*(z_m, z_k, r_k, -t) \\ &= \mathscr{F}^{-1}\{G(z_m, z_k, r_k, f)G^*(z_m, z_k, r_k, f)\}, \\ g_b(z_k, z_n, r_k, t) &= g(z_k, z_n, r_k, t) * g^*(z_k, z_n, r_k, -t) \\ &= \mathscr{F}^{-1}\{G(z_k, z_n, r_k, f)G^*(z_k, z_n, r_k, f)\}. \end{aligned} \tag{5}$$

When dealing with target detection problem in a multiple scatterers environment, the singular value decomposition (SVD) of first SRA received signal's auto-correlation matrix can be used to resolve the dominant scatterers. Here, we just use one element, that using mth element for instance, as an initial source, the received signal degenerates as $\mathbf{P}(z_m, f)$

$$\mathbf{P}(z_m, f) = \sum_{k=1}^{K} S(f)G(z_m, z_k, r_k, f)A_k(f) \times \mathbf{G}(z_k, \mathbf{z}_{SRA}, r_k, f) + N(z_n, f), \tag{6}$$

and its auto-correlation matrix $\mathbf{R}(f)$ is

$$\begin{aligned} \mathbf{R}(f) &= \mathbf{P}(z_m, f)\mathbf{P}^H(z_m, f) = \mathbf{U}(f)\mathbf{\Sigma}(f)\mathbf{V}^H(f) \\ &= \mathbf{U}_{tgt}(f)\mathbf{\Sigma}_{tgt}(f)\mathbf{V}^H_{tgt}(f) + \mathbf{U}_{int}(f)\mathbf{\Sigma}_{int}(f)\mathbf{V}^H_{int}(f). \end{aligned} \tag{7}$$

As shown in (7), the auto-correlation of signals consists of a space spanned by targets of interest, $\mathbf{\Sigma}_{tgt}$, and a space originated from interference, $\mathbf{\Sigma}_{int}$. Thus, an ITR or DORT procedure can be applied to selectively focus on the targets of interest after an appropriate analysis.

B. TR-MIMO detection

MIMO sonar detection is based on diversity exploitation. In TR-MIMO detection, waveform diversity and spatial diversity are considered by deploying multiple SRAs. Orthogonal waveforms can alleviate mutual interference between arrays, but a complicated transmit signal probably suffers more severe distortion in underwater acoustic channel. In our present detection system, orthogonal pulse continuous waves (PCW) are used as probe signals. Signals transmitted and received on the same SRA are discussed as above. For signals transmitted from a M-element SRA but received by another N-element SRA, the received signal becomes

$$P(z_n, f) = \sum_{m=1}^{M} \sum_{k=1}^{K} S_{TR}(z_m, f)G(z_m, z_k, r_k, f) \times G(z_k, z_n, r'_k, f) + N(z_n, f). \tag{8}$$

The phase of $G(z_m, z_k, r_k, f)$ in (8) is canceled out by its conjugation in $S_{TR}(z_m, f)$. This suggests that, for target localization in depth-range plane, a back-propagation approach can be adopted. If a TR-MIMO system has L SRAs, L^2 decisions are expected, where one SRA gets L approximately same depth-range results. The final decision gathers all preliminary decisions and gives the final output through data fusion algorithms, based on each SRA's coordinate.

In order to investigate the performance of TR-MIMO on target resolving, we perform a simple simulation using normal mode method [8] in a range independent environment. The environment parameters and system configuration are according to the lake experiment in III-A. In the simulation, two 8-element SRAs are set 14 m away from each other. SRA1 is 82 m away from a 10.55-m depth target, while SRA2 is 84 m separated from the same target. The simulation process is, firstly each SRA uses the element whose depth is nearest to the target's depth, to send its own probe signal; then each SRA receives its own echo, time reverses and sends it; finally received by all arrays and gives the localization results. If we set a origin of Cartesian coordinate for the detection system, for example an origin between SRA1 and SRA2, we can calculate the coordinate of a target of interest by using least square fitting. We omit this fusion problem, and simply verify the localization performance by checking the mainlobe of energy distribution.

The simulation results are shown as Fig.1. Here we just display the energy distribution and contour figures of two cases: 1) a 6 kHz PCW signal transmitted from SRA1 and received by SRA2 (Fig.1(a) & Fig1(c)), and 2) a 9 kHz PCW signal emitted from SRA2 and recorded by SRA1 (Fig.1(b) & Fig1(d)). The results verify that TR-MIMO has the ability to resolve a target. As mentioned in [9], the foci size of a time reversal mirror (TRM) can be approximately decided by the depth of waveguide D, and the modes propagating in that

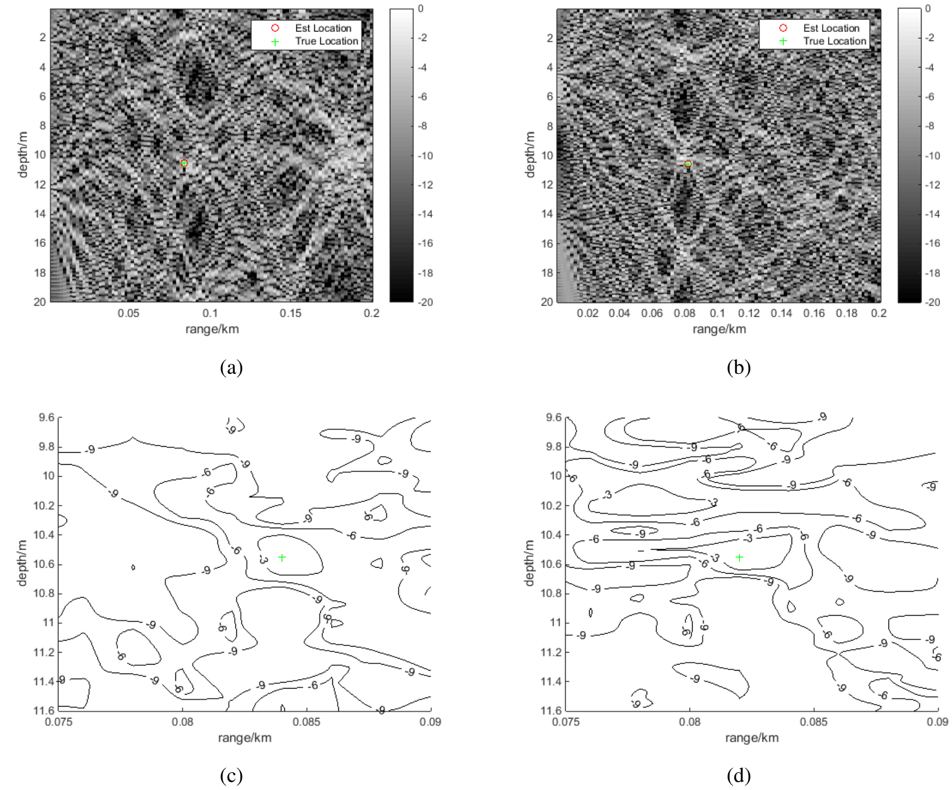

Fig. 1. Simulation results of TR-MIMO detection (target depth is 10.55m). Case I: a 6 kHz PCW signal transmitted from SRA1 and received by SRA2 (the range from target to SRA2 is 84 m).(a) Energy distribution. (c) Contour plot. Case II: a 9 kHz PCW signal emitted from SRA2 and received by SRA1 (the range from target to SRA1 is 82 m).(b) Energy distribution. (d) Contour plot.

waveguide,

$$\Delta_Z \sim \frac{D}{M}, \qquad \Delta_R \sim \frac{2\pi}{k_1 - k_M}, \tag{9}$$

where M is the numbers of effective modes, and k_1, k_M are the horizontal wavenumber of the first and last effective modes respectively. According to (9), the foci size should be Δ_Z ~0.26 m in depth, Δ_R ~2.45 m in range at 6 kHz and $\Delta_Z \sim$ 0.20 m, Δ_R ~1.90 m at 9 kHz, in a 20 m depth shallow water waveguide, which is a similar size shown in Fig.1(c) as Δ_Z ~0.26 m,Δ_R ~2.5 m, but a dispersive size in Fig.1(d) as Δ_Z ~0.23 m,Δ_R ~6 m. One should notice that, these are cases where signals are transmitted and received by different SRAs, the energy distribution is rather dispersive (There shows many speckle sidelobes in both results.). Also, the results of one SRA's own transmission and record are evaluated, but not displayed in this paper.

III. Experiment

In this section, the experiment was conducted in December, 2013. This lake experiment consists of focus verification test and the main TR-MIMO detection experiment.

A. Environmental Setup

Sound speed profile (SSP) around experiment area was measured by a conductivity-temperature-depth (CTD) casted on the research vessel (RV) before experiments. The measurement results depicted as Fig.2(a) suggest a nearly constant sound velocity with slightly positive gradient. The final sound speed profile (SSP) (Fig.2(b) red line) for propagation model computation is curve fitted through 9-order polynomial fitting method based on the up-cast period measurement. The estimated environmental parameters are collected in Fig.2(c). We assumed the experimental area was a flat region and a range independent environment.

Fig.3 shows the schematic view of equipment configurations. Two 8-element SRA were 14.4 m separated from each other. Each SRA had a 2-m inter-element spacing. SRA1 spanned from 1.4 m to 15.4 m, while SRA2 covered depth from 1.24 m to 15.24 m. SRA1's elements were numbered as Channel (Ch.) 1 to Ch. 8 from surface to bottom, and the same way numbered Ch. 9 to Ch. 16 for SRA2. A hollow stainless steel cylinder with 0.2 m in diameter and 1.5 m in length was set as a target at 10.57 m depth. In the first focus test, a transmit transducer replaced the target as a probe source (PS), and a 16-element receive vertical linear array (VLA) was used to monitor the focus quality. The 1 m inter-spaced VLA spanned from 1.8 m to 16.52 m as recorded by

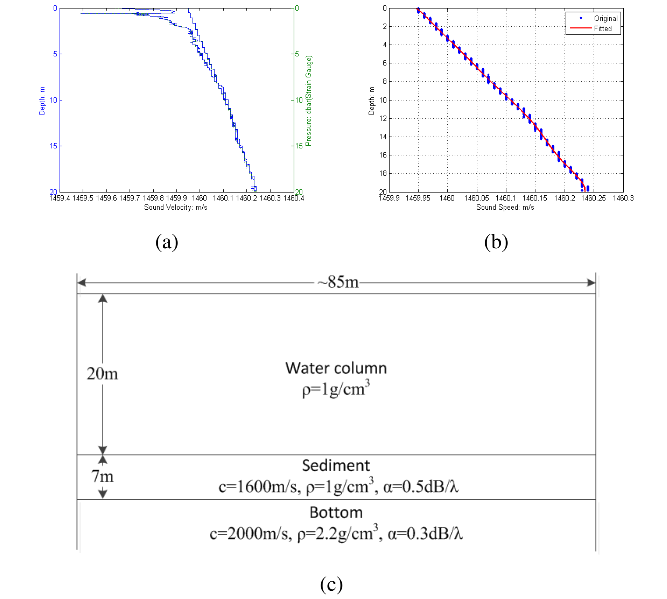

Fig. 2. Measured parameters. (a) Full cast measurement results (average salinity: 0.04935 PSU; mean temperature: 13.19 degree Celsius). (b) Sound speed profile acquired from up-cast data. (c) Diagram of environmental parameters.

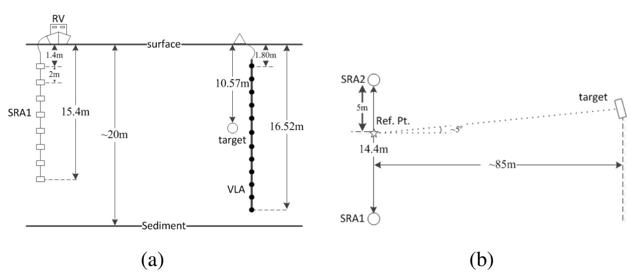

Fig. 3. Schematic view of system configuration. (a) Side view. (b) Top view.

2 temperature-depth recorder (TDR), meaning VLA was in a slightly tilt state. PS and VLA weren't deployed during TR-MIMO detection experiment.

B. Focus Test

To verify the performance of source-receive arrays (SRA), and its possibility of focus on some ranges, a focus experiment was conducted first at afternoon. A PS was set at 10.57 m in depth, and about 80 m away from the RV. First, PS sent a 10 ms Hanning windowed 7 kHz PCW signal. Then both SRAs transmitted their time reversed echo back for focus verification. Fig.4 shows the results of focus test. Fig.4(a) and 4(b) are PS's emission recorded by SRA1 and SRA2 respectively, indicating that the experiment area was a rich multi-path waveguide. The Ch. 9 in SRA2 didn't work and was dropped from time reversal transmission. The focus quality measured by VLA shown in Fig.4(c) and 4(d). The foci appeared at Ch. 10 around 0.1 sec in the figures. Still, energy got some dispersion at other depth. This test verified that SRAs could illuminate the target through time reversal by some echo analyses.

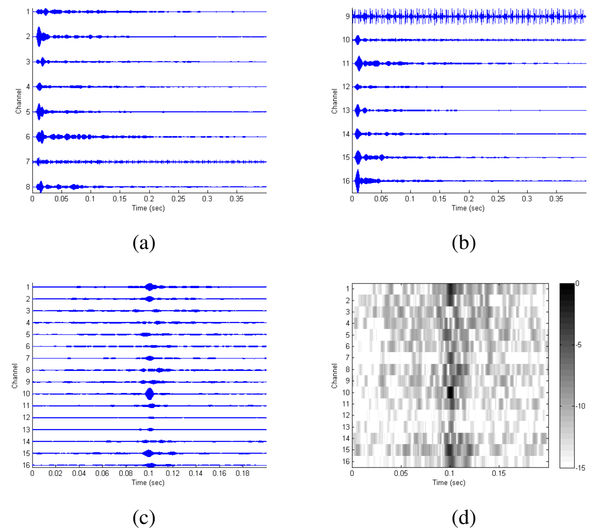

Fig. 4. Results of focus test. PS sent a 10 ms windowed 7 kHz signal and time reversed signals were received by VLA. (a) PS's signal received SRA1. (b) PS's signal received SRA2. (c) SRA2's time reversal transmission recorded by VLA. (d) Energy distribution of SRA2's transmission.

C. TR-MIMO Detection Experiment

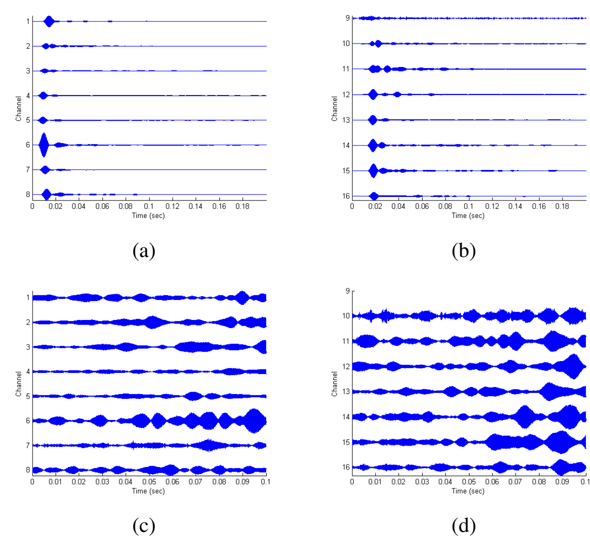

Fig. 5. SRAs' received echoes and their time reversal transmit waveforms. (a) 7 kHz echoes received by SRA1. (b) 9 kHz echoes recorded by SRA2. (c) SRA1's 7 kHz TR transmit signals. (d) SRA2's 9 kHz TR transmit signals.

Before experiments in the night, the target was set 85 m away from RV and 10.57 m in depth as Fig.3. TR-MIMO detection experiment was carried out as following steps: 1) Use a transducer, which was set 1 m beside SRA1 (13.4 m to SRA2) and 10 m below water surface, first sent a 10 ms Hanning windowed 7 kHz PCW signal, then emitted a 10 ms Hanning windowed 9 kHz signal. 2) SRA1 used the 7 kHz echo for time reversal transmission, while SRA2 used the 9 kHz one. 3) SRAs gave the final decisions. For off-line computation, the searching step is 0.01 m in depth and 2 m

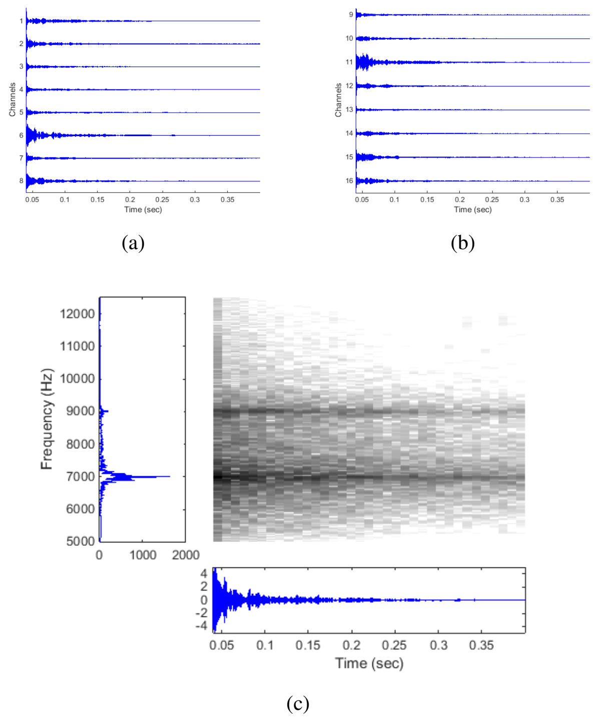

Fig. 6. Received signals at time reversal transmission step. (a) SRA1's final received signals. (b) SRA2's final received signals. (c) Time and frequency analysis of signal recorded on Ch. 6.

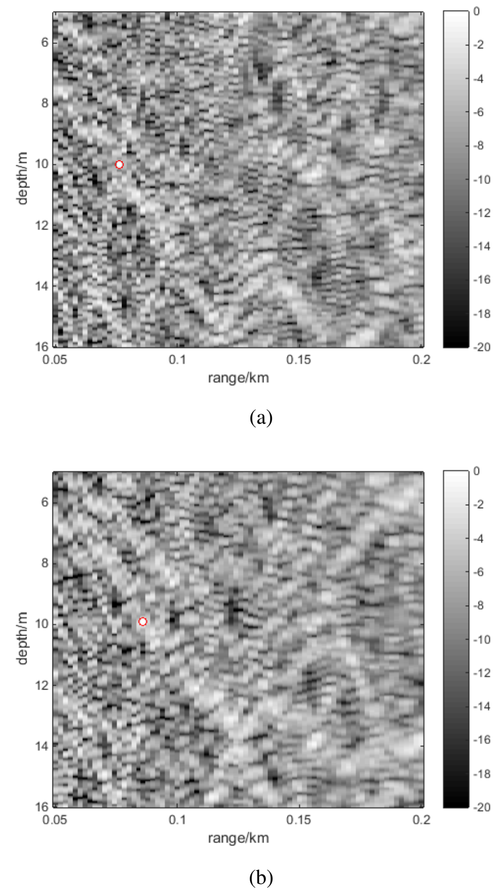

Fig. 7. Detection results (the parameters in brackets are the energy peak position marked by red circle in figures). (a) The detection result of SRA1 based on 9 kHz signal (depth: 10 m; rang 76 m). (b) The detection result of SRA2 based on 7 kHz signal (depth: 9.91 m; rang 86 m).

in range.

Because there might exist a stable focus period, the broadside transmission echoes were simply analyzed using correlation method for real-time data acquisition consideration. Echoes in the first step are shown in Fig.5(a) (recorded by SRA1) and Fig.5(b) (recorded by SRA2). The first and highest peaks in each channel are direct blast from the transducer and peaks in SRA2's plot show some time lag for SRA2 had more distance away from the source. After analysis and extraction, the time reversal waveform for each SRA are depicted in Fig.5(c) and 5(d). Therefore, the final echoes (as Fig.6) of each array contain the two frequency components as figured out in Fig.6(c) by taking Ch.6 for instance. One can see that 9 kHz component contributes a considerably low return energy. Also, 9 kHz component is not a dominant part in channels of SRA2 and will be discussed in the next part. The decisions given by the highest peak of each array impose a huge divergence. Only, SRA2 using 7 kHz signal gives a convincing localization result (Fig.7(b)), while others give a total miss as SRA1 using 9 kHz signal (Fig.7(a)). But searching the second or third energy peaks, we correct the results that: SRA1 uses 7 kHz signal estimates 10.19 m in depth, 84 m in range; using 9 kHz gives 9.59 m in depth, 86 m in range. SRA2 using 9 kHz gives 9.94 m in depth and 84 m in range. The focus quality is similar to the simulation as Fig.1(c) and 1(d). The final decision is first to calculate each SRA's mean result, then to determine the final estimation by equipments' geometric relation.The final result is (-2.4, 84, 9.90) m in (x, y, $Depth$) coordinate relative to the reference point in Fig3(b).The ground truth was (5.4, 85, 10.57) m, whose geography location was measured by GPS and depth was recorded by TDR.

D. Discussion

The experiment successfully resolved a target with a final reliable estimation through diversity gains. We still believe TR-MIMO method could give a better result. The two SRAs had to be deployed on the same RV, which gives up target's angle diversity and can't diminish some biases. In the experiment, a more robust focus and interference rejection could have improved our detection system, if we had adopted a subspace decomposition or other further analyses. Still, our detection procedure can evolve to an iterative one for further improvement. Moreover, in the focus test, it showed some energy diffused to other depth which might be caused by the signal distortion at SRA, leading to a energy dispersion. Also, an environmental parameter mismatch could contribute to difference between model prediction and field measurement.

IV. Conclusion

Interference suppression and depth-range focus can be achieved by using TR method, while the MIMO structure provides some kinds of diversities for detection performance enhancement. In this paper, we propose a TR-MIMO detection method, making the TR approach and MIMO detection framework as complementary for each other. By deploying multiple SRAs, we try to focus transmit energy as well as exploiting spatial and waveform diversity. In a preliminary experiment, the detection system using 2 SRAs figures out the target with a reliable estimation. Though the final result gives a little bias, the system still shows the ability of a reliable detection result under constraints and environmental mismatch. TR-MIMO method will give better results when applied more sophisticated processing approaches.

Acknowledgment

The paper is supported by the National Natural Science Foundation of China. (No. 61171148).

References

[1] H. Song, W. S. Hodgkiss, W. A. Kuperman, K. Sabra, T. Akal, and M. Stevenson, "Passive reverberation nulling for target enhancement," *The Journal of the Acoustical Society of America*, vol. 122, no. 6, pp. 3296–3303, 2007.

[2] C. F. Gaumond, D. M. Fromm, J. F. Lingevitch, R. Menis, G. F. Edelmann, D. C. Calvo, and E. Kim, "Demonstration at sea of the decomposition-of-the-time-reversal-operator techniquea)," *The Journal of the Acoustical Society of America*, vol. 119, no. 2, pp. 976–990, 2006.

[3] F. D. Philippe, C. Prada, M. Fink, J. Garnier, and J. de Rosny, "Analysis of the time reversal operator for a scatterer undergoing small displacements," *The Journal of the Acoustical Society of America*, vol. 133, no. 1, pp. 94–107, 2013.

[4] K. Raghukumar, B. D. Cornuelle, W. S. Hodgkiss, and W. A. Kuperman, "Pressure sensitivity kernels applied to time-reversal acoustics," *The Journal of the Acoustical Society of America*, vol. 124, no. 1, pp. 98–112, 2008.

[5] J. M. Aughenbaugh, B. R. La Cour, and J. M. Gelb, "Interference mitigation for multistatic active sonar," *Oceanic Engineering, IEEE Journal of*, vol. 40, no. 3, pp. 570–582, 2015.

[6] T. Yang, "Detection capacities of distributed and centralized systems: A comparative study," *Oceanic Engineering, IEEE Journal of*, vol. 40, no. 3, pp. 666–682, 2015.

[7] Y. Pailhas and Y. Petillot, "Large mimo sonar systems: a tool for underwater surveillance," in *Sensor Signal Processing for Defence (SSPD), 2014*. IEEE, 2014, pp. 1–5.

[8] M. B. Porter, "The kraken normal mode program," DTIC Document, Tech. Rep., 1992.

[9] S. Kim, W. Kuperman, W. Hodgkiss, H. Song, G. Edelmann, and T. Akal, "Robust time reversal focusing in the ocean," *The Journal of the Acoustical Society of America*, vol. 114, no. 1, pp. 145–157, 2003.